Article

Proof-of-Concept Study on Supercritical Fluid Chromatography Hyphenated with a Fast Optoelectronic Nose for Online Monitoring of Odorant Molecules

Cyrille Santerre [1,*] **, David Touboul** [2] **, Thierry Livache** [3] **and Cyril Herrier** [4]

1   Institut Supérieur International du Parfum, de la Cosmétique et de l'Aromatique Alimentaire (ISIPCA), 34-36 Rue du Parc de Clagny, F-78000 Versailles, France
2   Laboratoire de Chimie Moléculaire (LCM), Centre National de la Recherche Scientifique (CNRS) UMR 9168, Ecole Polytechnique, Institut Polytechnique de Paris, F-91120 Palaiseau, France
3   Université Grenoble Alpes, Commissariat à l'Énergie Atomique (CEA), Centre National de la Recherche Scientifique (CNRS), Grenoble Institut d'Ingénierie et de Management (INP), Institut de Recherche Interdisciplinaire de Grenoble (IRIG), Systèmes Moléculaires et nanoMatériaux pour l'Énergie et la Santé (SyMMES), F-38000 Grenoble, France
4   Aryballe, F-38000 Grenoble, France
*   Correspondence: csanterre@isipca-lafabrique.fr

Abstract: In this study, we explored the use of surface plasmon resonance (SPR) and Mach–Zehnder interferometry for detecting compounds in complex mixtures separated by supercritical fluid chromatography. Each molecule was individually injected and analyzed by supercritical fluid chromatography (SFC) in a 10% alcoholic solution. The fingerprints obtained via the sensors were then compared to the fingerprints of the same molecules present in a lemon essential oil (EO) at the same dilution. The results show a remarkable correlation between UV sensors and electronic noses (e-nose), enabling compound detection. The obtained signals are normalized and presented as radar charts to visualize the specific olfactory signatures of each molecule. The olfactory profiles of monoterpenes $C_{10}H_{16}$ such as α-pinene and limonene show notable differences, as do the $C_{10}H_{16}O$ isomers (citral, geranial, and neral). Mach–Zehnder interferometry also allows for the discrimination of limonene enantiomers, a challenging task for current chromatography techniques. Statistical analysis confirms the ability of these technologies to differentiate compounds, including isomers. Even if UV detection is more sensitive than SPR, e-noses (SPR and Mach–Zehnder interferometers) offer the unique advantage of providing specific signatures for each compound, facilitating real-time identification. This study demonstrates the effectiveness of combining e-noses with SFC for rapid, non-destructive detection of volatile compounds. This concept can be extended to other terpenoids and volatile compounds, and hybridization with gas chromatography could be a future potential development.

Keywords: supercritical fluid chromatography; olfactometry; surface plasmonic resonance; Mach–Zehnder interferometry; odorant molecule

1. Introduction

An odor is composed of a single or complex mixture of volatile compounds that are present in concentrations above the human perception threshold [1]. Olfactometry is related to all techniques that use sensors to detect and evaluate volatile compounds eluting from a chromatographic system. Olfactometry (O) coupled with a chromatographic

method of detecting volatile molecules, such as gas chromatography (GC), brings an undeniable advantage for the identification of sulfur and nitrogen volatile molecules and is complementary to other detection methods, such as flame ionization detection (FID) or mass spectrometry (MS), for example [2,3].

Currently, other greener separation techniques such as supercritical fluid chromatography (SFC) are booming and allow the separation of both volatile and non-volatile organic compounds [4–7]. The supercritical state was discovered by the French physicist Cagniard de Latour in 1822. For carbon dioxide (CO_2), the most used molecule in the supercritical state today, the critical point is reached at 31 °C and 74 bar. Most of the physical-chemical properties of a substance in the supercritical state are close to that of the gaseous and/or liquid state. For example, density and diffusivity are close to those of the liquid states, whereas viscosity is similar to the gaseous one. SFC can be coupled with different detectors, such as evaporative light scattering detectors (ELSD) [8], diode array detectors (DAD) [9], nuclear magnetic resonance (NMR) [10], or mass spectrometry (MS) [11].

Nevertheless, contrary to FID for GC, few sensors hyphenated with SFC can be considered as universal. Some articles are available in the literature on coupling with Charged Aerosol Detectors (CAD) [12,13] but leading to poor physicochemical information. It is crucial to acquire as much chemical data as possible in order to annotate the molecules present in an extract or an odor during the dereplication process. However, in the case of coupling with SFC, direct detection by human noise methodology is significantly complicated. In fact, even if CO_2 is odorless, its toxicity by inhalation makes direct coupling impossible [14]. To overcome this obstacle, a possible solution would be to use air as make-up gas to dilute the sample in the gas phase and thus make it breathable. According to the literature [15], if the level of CO_2 in the make-up air stream is less than 0.1%, the panelist will be at no risk of olfaction. This means dilution by 1000 of the sample. However, the dilution factor will directly decrease the detection threshold of the volatile molecules. This dilution factor is made up of several steps, the first of which involves splitting the flowrate to limit the amount of gas sent to the sensor. The second step involves decompressing the CO_2 from the supercritical to the gaseous state, leading to a large expansion of the gas (expansion factor close to 500). And finally, the final step is the complicated transport of these molecules in a mixture of moist air and gaseous CO_2, avoiding precipitation.

In recent years, the development of electronic noses has been growing. These devices make it possible to smell under extreme conditions without toxicity constraints [16]. A lot of examples of coupling between GC and e-noses describe systems for which the e-nose measurements are not real-time like those of classical detectors (FID, DAD). For example, a cold trap can be used to catch and release selected parts of the eluent getting out of the GC column [17]. Only one measurement with the e-nose is made per trapped section, since one measurement needs at least a few min.

In this preliminary study, we studied the feasibility of coupling a fast opto-electronic nose based on two technologies: first on the principle of surface plasmonic resonance (SPR) [18–20] and second on the principle of Mach–Zehnder interferometry [21,22].

The typical SPR device comprises a polarized light source, a prism, a metal layer (often gold), and a detector. Polarized light passes through the prism and is projected onto the metal layer at the interface between two media of different refractive indices. When the polarized light reaches the metal layer at a specific angle, it excites free electrons on the metal surface, creating surface plasmons. This excitation occurs at a precise resonance angle, where the intensity of the reflected light decreases significantly.

The metal surface is functionalized with specific receptors that can bind the analytes of interest. When the analytes bind to the receptors, they change the local refractive index at the metal surface. This change in refractive index leads to a variation in the resonance

angle, which is detected and measured by the SPR system. Changes in resonance angle are recorded in resonance units (RU). A typical SPR signal shows a rapid increase when the analyte binds to the receptor, followed by a plateau phase when equilibrium is reached, and finally, a decrease when the analyte dissociates. These data make it possible to quantify molecular interactions, such as dissociation constants and binding kinetics.

The Mach–Zehnder interferometer is an optical device that uses two semi-reflecting and two full mirrors to split and recombine a coherent light beam. The light beam is first split into two distinct paths by a semi-reflecting mirror. The two beams follow different paths before being recombined by a second semi-reflecting mirror. During splitting, each beam can interact with molecules present in the environment. These interactions slightly modify the phase of the light beams, depending on the properties of the molecules encountered. When the beams are recombined, the phase differences create constructive or destructive interference, producing an interference pattern that can be analyzed.

In the context of electronic noses, light beams pass through functionalized sensors that react specifically to certain volatile compounds. The phase changes induced by these interactions are detected and analyzed to identify the compounds present. The interference patterns obtained are unique for each type of molecule, enabling precise identification.

One of the main advantages of the Mach–Zehnder interferometer is its high sensitivity. It can detect very small phase changes, making it ideal for detecting traces of volatile compounds. What's more, it enables real-time, label-free analysis, which is crucial for applications such as perfumery, cosmetics, and flavors.

These noses were hyphenated with an SFC system for the detection of odorous compounds, such as monoterpenes (limonene, α-pinene) and oxygenated monoterpenes (neral, geranial) families. The high frequency of images acquisition, i.e., up to 60 Hz, allows for real-time monitoring and analysis of the eluted composition getting out of the SFC.

2. Materials and Methods

2.1. Sample Preparation

The different mixtures of diluted compounds were composed of S-limonene, R-limonene, α-pinene, and citral (from Sigma-Aldrich, Saint-Quentin-Fallavier, France). Citral is an isomer mixture composed of geranial and neral. The lemon essential oil (*Citrus limon* (L.) Burm. F.) from Italy was supplied by Payan Bertrand (Grasse, France). Each of the pure compounds and EOs were diluted to 10% w/w in absolute ethanol (from Sigma-Aldrich, Saint-Quentin-Fallavier, France) suitable for HPLC.

2.2. SFC Parameters

The full setup is introduced in Figure 1. SFC-UV experiments were performed on a 1260 Infinity Analytical System (Agilent Technologies, Santa Clara, CA, USA) consisted of a SFC binary pump, a degasser, a SFC autosampler with a 5 µL loop, an Aurora SFC Fusion ™ A5 module, and a column oven compartment. Detection was performed using a diode array detector (DAD) at a fixed wavelength of 210 nm $\pm$ 4 nm (reference 360 nm $\pm$ 10 nm), and an acquisition frequency of 1.25 Hz. Instrument control and data collection were carried out using MassHunter Workstation software (B.10.00, Agilent Technologies, USA).

Two columns in a series were used for chromatography, i.e., a Hypercarb$^{\circledR}$ (150 mm $\times$ 4.6 mm, 5 µm, Thermo Scientific, Waltham, MA, USA) and a Poly-(butylene terephthalate) DCpack PBT (150 mm $\times$ 4.6 mm, 5 µm, DAICEL Corporation, Osaka, Japan). The mobile phase consisting of 100% CO_2 was used at a flowrate of 1.5 mL/min. The column temperature was kept at 40 °C and a backpressure (BPR) gradient was defined from 90 to 250 bar in 14.5 min.
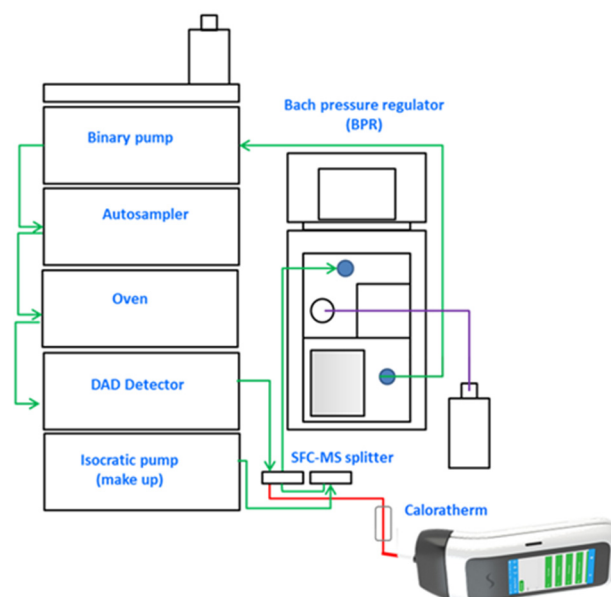
Figure 1. Hyphenated setup between SFC and the optoelectronic nose.

2.3. SFC-E-Nose Hyphenation

An SFC-MS Splitter Kit G4309-68715 (Agilent Technologies, USA) was used in order to divide the flow sent to the sensor (about 1/3 to the sensor and 2/3 to the BPR). The restriction capillary was 50 µm ID × 1 m length (red line in Figure 1). For the hyphenation with e-noses, a caloratherm (Selerity Technologies Inc., Salt Lake City, UT, USA) was installed and set at 80 °C.

The variation of the total flow rate of CO_2 after expansion towards the binary flowrate was determined (Figure 2). The limit of our gas flowmeter's maximum flow measurement restricted us to the 90 to 140 bar pressure range we were able to study. A linear relationship was determined, and the experiments indicate that an expansion factor of 400 is achieved at an SFC flowrate of 1 mL/min. This value must be taken into account for the optimization of the hyphenated system between SFC and an e-nose.
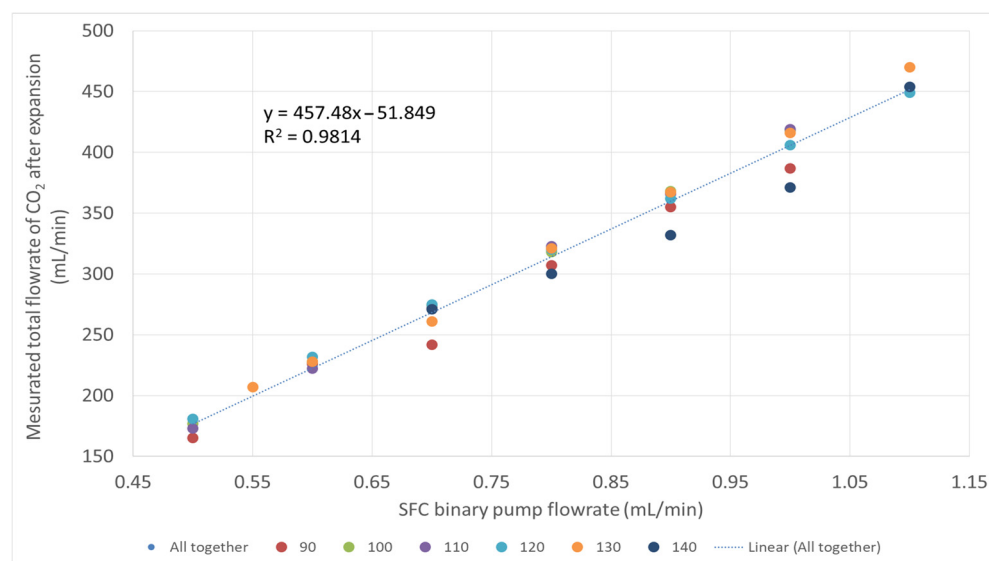

Figure 2. Cumulative flowrates measured at the capillary outlet "To E-Nose" and "To BPR" as a function of the flowrate of the SFC and BPR pressure used in the system (90–140 bar, colored spots). The solvent is pure CO_2, and the temperature in the column oven is 40 °C.

The value of the slope of this straight line therefore represents the expansion factor of supercritical CO_2 as it changes state (Figure 2). This factor is 400, which means that when the SFC flowrate is 1 mL/min, the measured flowrate of the same compound after expansion to atmospheric pressure will be 405.6 mL/min.

2.4. E-Nose Parameters

E-nose measurements were obtained from a NeOSePro V1 (Aryballe, Grenoble, France) composed by an SPR sensor engaging an array of 47 different functional sensing areas. Data were recorded at a framerate of 4 Hz, and from a NeOse Advance (Aryballe, France) composed by an array of 64 functional MZI sensors integrated in a photonic silicon chip. Both devices also embedded a temperature and humidity sensor. The pumping system of the devices were disabled because flowrate is monitored by the SFC system. The normalized data were reprocessed by calculating the covariance matrix, which enabled us to understand the relationships between the different variables. An eigenvalue decomposition of the covariance matrix was then performed to obtain the eigenvectors and eigenvalues. The eigenvectors represent the new dimensions (principal components), and the eigenvalues indicate the importance of each dimension.

3. Results

3.1. SPR Detection

First, each compound of the mixture was recorded individually with the detectors based on the principle of surface plasmonic resonance (SPR). Simultaneous recording of the UV sensor and the e-nose showed remarkable synchronicity. Detection of the different compounds was obtained by the UV sensor in the dense SFC phase (Figure 3), and signal correlations between UV and SPR sensors in terms of retention time can be observed (Figure 3). On the sensorgrams, each colored curve represents the signal from one of the sensors in the e-nose (Figure 3).
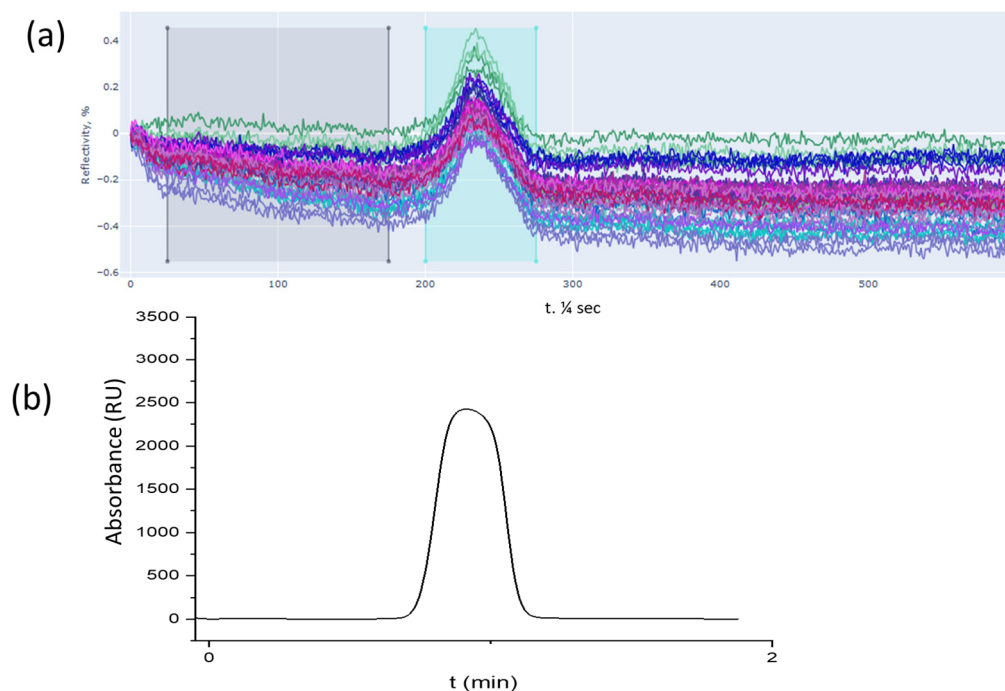

Figure 3. Simultaneously acquired UV chromatograph (**b**) and e-nose sensorgram (**a**) at the outlet of the split eluent with 10% α-pinene outgoing from SFC. In (**a**), each color represents the signal from one of the biosensors.

For a second time, the sensorgrams are then transposed into radar chart [23] form for visual comparison. For example, for α-pinene molecules, the raw data in Figure 3a are then transposed into radar chart and visualized in Figure 4a.
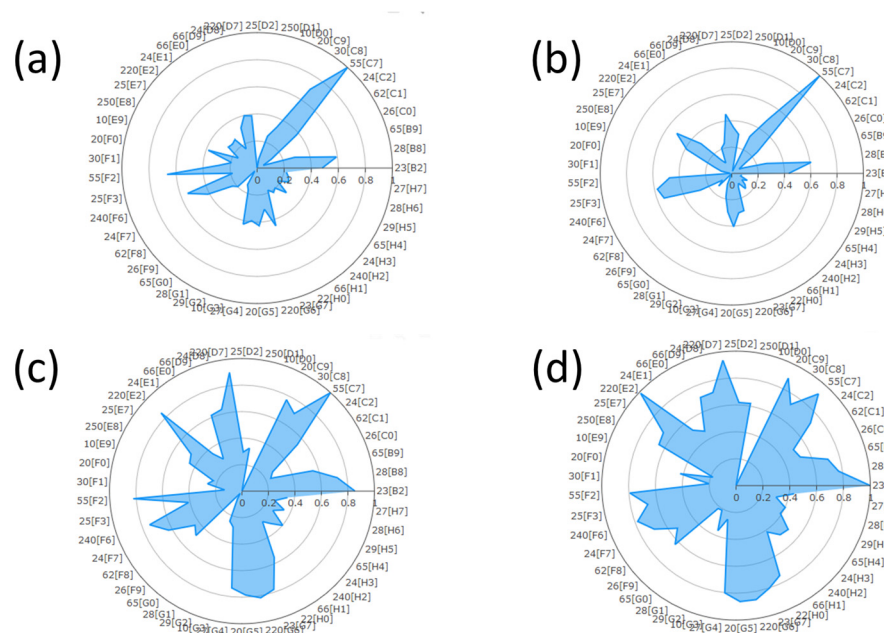

Figure 4. Radar chart at the outlet of the split eluent with 10%: (**a**) α-pinene, (**b**) R-limonene, (**c**,**d**) citral isomers (neral and geranial).

E-nose sensors allow the device extract signatures for compound identification, and the method of extraction can be adapted from Maho et al. [24]. Briefly, a signature for a measurement is obtained by subtracting the signal of the baseline from signals of the detected molecules for each sensor. If a baseline correction is performed at the beginning of the acquisition, the signal is directly readable for each sensor when molecules are detected. These signals are proportional to the injected quantity of each molecule. In order to obtain a unique signature independent of the quantity of a volatile organic compound (VOC), the signals are normalized and depicted with a scale between 0 and 1 for the minimum and maximum signal, respectively. This normalized signature is presented as a radar chart for which each radius corresponds to the normalized signal of each functionalized sensor. This figure allows us to evaluate the relative chemical affinity of each sensor towards the detected molecule. This leads to a specific pattern, also called "olfactive signature".

Radar charts of the olfactory signatures for several standards have been produced (Figure 4). A visual comparison of the two graphs obtained between limonene and α-pinene (Figure 4a,b), which both belong to the monoterpene family, reveals a notable difference in profile. The same results were obtained with citral isomers, i.e., neral and geranial (Figure 4c,d). Moreover, significant differences between monoterpene signatures and oxygenated monoterpenes were enlightened. Therefore, functionalized SPR technology is able to differentiate various VOCs bearing small structural differences.

The sensitivity of the presented sensor seems to be very different. In the presented data, the SPR S/N is 0.4/0.1 = 4, when for UV SNR, it is 2500/1 = 2500. It must be noted that a UV detector has the advantage of being in the dense CO_2 phase, when the e-nose detection occurs in the expanded gas phase but allocates a unique signature for each compound. Thus, an e-nose can be employed to recognize the compounds of complex mixtures separated by SFC, after a learning phase

3.2. Mach–Zehnder Detection

Sensorgrams based on the principle of Mach–Zehnder interferometry are obtained and transposed in the form of radar charts. Figure 5 shows the graphs for all the compounds studied with this technique. Here, the radar charts are L2-normalized, changing the scale compared to SPR. L2 normalization of data for a radar chart is a common method of making data comparable across different dimensions. This technique involves dividing each value by the L2 norm (or Euclidean norm) of the data vector. This transforms each data point into a unit vector, enabling values to be compared on a common scale.
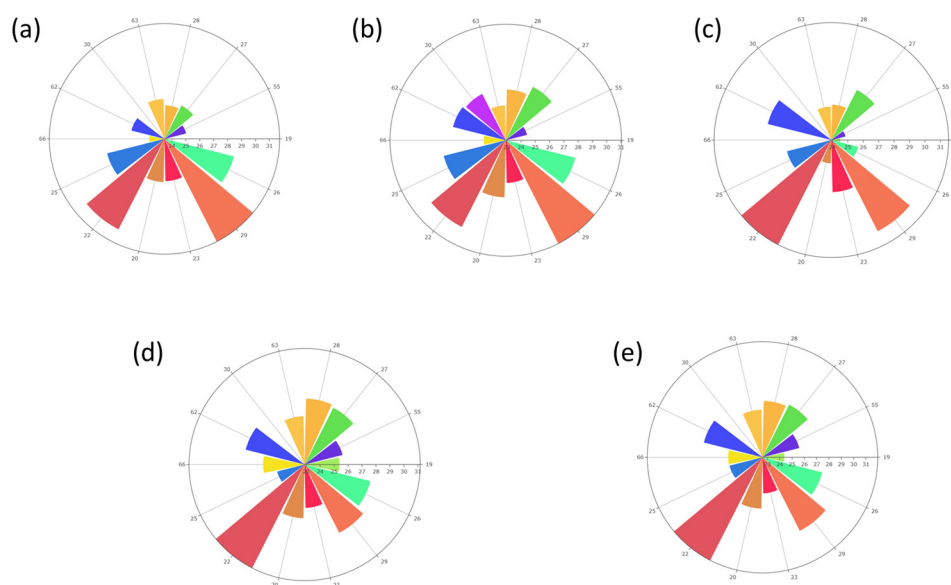

Figure 5. Radar chart at the outlet of the split eluent with 10%: (**a**) α-pinene, (**b**) R-limonene, (**c**) S-limonene, (**d**,**e**) citral. In figures, each color represents a biosensors.

Similarly to SPR analysis, it is possible to discriminate between monoterpenes (Figure 5a–c), oxygenated monoterpenes (Figure 5d,e) and monoterpenes versus oxygenated monoterpenes. As with SPR technology [25], Mach–Zehnder interferometry is able to discern the enantiomers of limonene (Figure 5b,c) which remains a complicated task in terms of chromatography.

3.3. ACP Analysis

From the radar chart signature, statistical analysis of the data obtained using Mach–Zehnder interferometry (Figure 6) were performed. If we express the coordinates of the different compounds along the different axes as follows [PCA1, PCA2], the following results are obtained: α-pinene [−1.0, −1.8], R-limonene [−1.3, +2.0], and S-limonene [+2.6, −0.9], while citral has two isomers (citral and geranial) so two peaks appear on the SFC chromatogram: isomer number 1 (first retention time) [+3.3, 0.0], citral isomer number 2 (second retention time) [+2.8, −0.3], α-pinene in essential oil [−1.6, −2.3]. For α-pinene alone or in essential oil, we used the midpoint between the three injections as coordinates. A difference between the two monoterpenes (α-pinene and R-limonene) was revealed on axis PCA 2 (24.5%), and a similarity on axis PCA 1 (49.4%). This confirms that these molecules are close but with small differences detectable by this technology. For the comparison between one of the citral compounds (second peak) and α-pinene peaks, the analysis shows a large difference on two axes, PCA 1 and PCA 2. These molecules are therefore clearly differentiable by this detector. For the comparison between two enantiomers R-limonene and S-limonene, the analysis shows a large difference on two axes, PCA 1 and PCA 2. These molecules are therefore clearly differentiable by this detector as

well. Now, if we look at an α-pinene component in lemon EO and the same compound as a pure standard, the statistical analysis shows a fairly small difference on axes PCA 1 and PCA 2, confirming that these two molecules belong to the same chemical family.
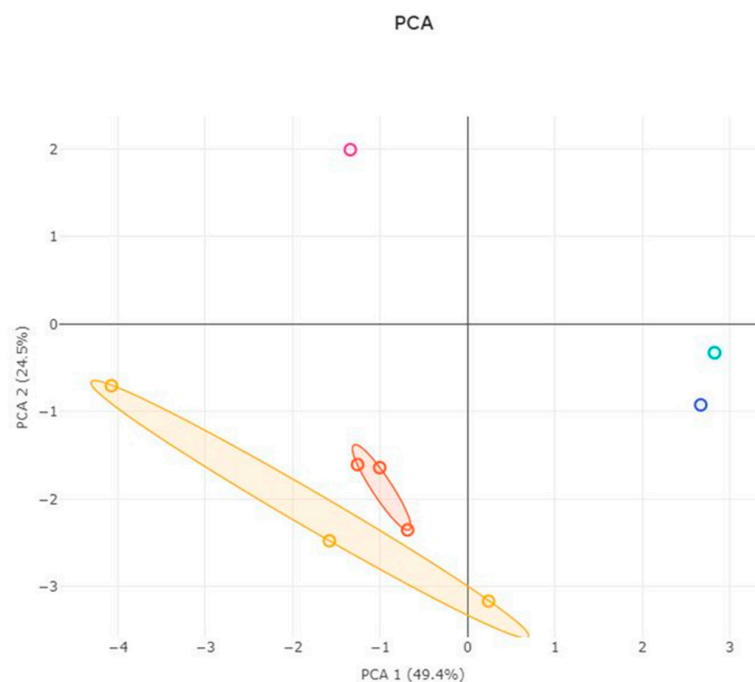

Figure 6. Principal component analysis of signatures obtained with the measurement of 4 different VOC: R-limonene (purple), S-limonene (blue), α-pinene (orange), citral isomer 2 (cyan), and α-pinene in essential oil of lemon (yellow).

4. Discussion

The results obtained from surface plasmon resonance (SPR) detection and Mach–Zehnder interferometry show a very interesting ability to differentiate volatile organic compounds (VOCs) with minimal structural differences. The synchronization of UV and SPR signals, as well as the transposition of sensorgrams into radar charts, allows for precise identification of compounds through their specific olfactory signatures [26]. Normalized olfactory signatures, presented in the form of radar charts, reveal notable differences between monoterpenes and oxygenated monoterpenes, as well as between citral isomers. These results are consistent with previous studies on SPR detection, which have demonstrated the sensitivity and precision of this technology for analyzing molecular interactions. Our findings align with those of previous studies that have utilized SPR technology for the detection and differentiation of VOCs. For instance, Jia et al. [27] demonstrated the effectiveness of SPR in distinguishing between various aromatic compounds, highlighting the technology's high sensitivity and specificity. Similarly, Cho et al. [28] reported the successful application of SPR in identifying subtle differences in the molecular structures of terpenes, which corroborates our observations regarding monoterpenes and oxygenated monoterpenes. The use of Mach–Zehnder interferometry further supports these findings, as illustrated by Roy et al. [29], who showed that this technique could effectively differentiate enantiomers of chiral molecules, a task traditionally challenging for chromatographic methods. The implications of these results are vast. The ability to accurately differentiate VOCs opens up prospects for applications in various fields, such as environmental monitoring, food safety, and clinical diagnostics [30,31]. SPR technology, combined with Mach–Zehnder interferometry, offers a robust method for real-time, label-free analysis of molecular interactions. In the perfumery industry, this capability allows for the precise

identification and differentiation of fragrance components, leading to the creation of more refined and unique scents. In cosmetics, the ability to monitor VOCs can enhance product formulation by ensuring the stability and consistency of aromatic compounds. In the flavor industry, detecting off-notes in food products can significantly improve quality control processes, ensuring the authenticity and desirability of flavors. Future research could focus on improving the sensitivity and specificity of SPR and Mach–Zehnder sensors. The integration of advanced plasmonic materials and nanostructures could enhance sensor performance [26]. Recent advancements in nanotechnology suggest that incorporating nanostructured materials can significantly boost the detection capabilities of SPR sensors, making them more responsive to minute changes in molecular interactions. Additionally, the application of machine learning for SPR data analysis could provide deeper insights and better interpretation of results. Machine learning algorithms, such as neural networks and support vector machines, have shown promise in analyzing complex datasets, enabling more accurate and faster identification of VOCs. Moreover, the development of hybrid models that combine machine learning with traditional analytical methods could further improve the robustness and reliability of VOC detection systems.

5. Conclusions

We present here the first hyphenation between SFC and an e-noses. The positive results of this proof-of-concept study provide an interesting basis for implementing this hyphenation on a larger scale in order to validate these preliminary results. Future tests will aim to evaluate the effectiveness of these sensors in recognizing a larger number of compounds and chemical families. Detection of components of a mixture has been compared between chromatographs obtained with UV absorption in the dense supercritical fluid phase and e-nose chromatographs obtained after expansion in the gas phase. Remarkable synchronicity of peak detection is observed in terms of retention time. The detection of the compounds is in relation to the sensitivity of each detector. The crucial advantage of these two optical e-nose technologies is their fast response, which allows them to distinguish events within a second. Another advantage of e-noses is the possibility to identify in real-time the compounds which are detected. Libraries can be created from the signatures of individual compounds. A comparative search using algorithms can then be used to identify the molecules in different media. The contribution of artificial intelligence to this identification process would also seem to be a very interesting next step. AI can be used in a number of ways. It will be able to extract data automatically from the sensorgram, which is currently performed manually. Secondly, machine learning algorithms, such as neural networks, can be trained to classify odors according to the signatures obtained by the electronic nose. This would enable a wide range of odors to be efficiently recognized and differentiated. Deep learning techniques will be able to detect complex patterns in olfactory data, enabling the discovery of non-obvious relationships between different odorant molecules. AI will also be able to help optimize the e-nose's sensor configuration by identifying the most relevant sensors for each type of odor, thus improving the device's accuracy and efficiency. Finally, using machine learning techniques, it will be possible to create and maintain databases of olfactory signatures, facilitating the comparison and identification of new or unknown odors.

Author Contributions: Conceptualization, C.S., D.T., T.L., and C.H.; methodology, C.S., D.T., and C.H.; software, C.S. and C.H.; validation, C.S., D.T., and C.H.; formal analysis, C.S., D.T., and C.H.; investigation, C.S. and C.H.; resources, C.S., D.T., T.L., and C.H.; data curation, C.S. and C.H.; writing—original draft preparation, C.S. and C.H.; writing—review and editing, C.S., D.T., T.L., and C.H.; visualization, C.S. and C.H.; supervision, C.S., D.T., and C.H.; project administration, C.S. and C.H.; All authors have read and agreed to the published version of the manuscript.

Conflicts of Interest: Author Cyril Herrier was employed by the company Aryballe. The remaining authors declare that the research was conducted in the absence of any commercial or financial relationships that could be construed as a potential conflict of interest.

References

1. Farré-Armengol, G.; Fernández-Martínez, M.; Filella, I.; Junker, R.R.; Peñuelas, J. Deciphering the Biotic and Climatic Factors That Influence Floral Scents: A Systematic Review of Floral Volatile Emissions. *Front. Plant Sci.* **2020**, *11*, 1154. [CrossRef]
2. Raffo, A.; Moneta, E.; Ferrari Nicoli, S.; Paoletti, F. GC-Olfactometric Characterisation of off-Odours in Commercially Packaged Rocket Leaves. *Food Packag. Shelf Life* **2020**, *25*, 100540. [CrossRef]
3. Isleten Hosoglu, M.; Karagul-Yuceer, Y.; Guneser, O. Aroma Characterization of Heterotrophic Microalgae Crypthecodinium Cohnii Using Solid-Phase Microextraction and Gas Chromatography–Mass Spectrometry/Olfactometry during Different Growth Phases. *Algal Res.* **2020**, *49*, 101928. [CrossRef]
4. Akbal, L.; Hopfgartner, G. Supercritical Fluid Chromatography–Mass Spectrometry Using Data Independent Acquisition for the Analysis of Polar Metabolites in Human Urine. *J. Chromatogr. A* **2020**, *1609*, 460449. [CrossRef] [PubMed]
5. Rice, J.; Lubben, A.; Kasprzyk-Hordern, B. A Multi-Residue Method by Supercritical Fluid Chromatography Coupled with Tandem Mass Spectrometry Method for the Analysis of Chiral and Non-Chiral Chemicals of Emerging Concern in Environmental Samples. *Anal. Bioanal. Chem.* **2020**, *412*, 5563–5581. [CrossRef]
6. Santerre, C.; Vallet, N.; Touboul, D. Fingerprints of Flower Absolutes Using Supercritical Fluid Chromatography Hyphenated with High Resolution Mass Spectrometry. *J. Chromatogr. B* **2018**, *1092*, 1–6. [CrossRef]
7. Huang, Y.; Tang, G.; Zhang, T.; Fillet, M.; Crommen, J.; Jiang, Z. Supercritical Fluid Chromatography in Traditional Chinese Medicine Analysis. *J. Pharm. Biomed. Anal.* **2018**, *147*, 65–80. [CrossRef]
8. Poulton, A.M.; Poulten, R.C.; Baldaccini, A.; Gabet, A.; Mott, R.; Treacher, K.E.; Roddy, E.; Ferguson, P. Towards Improved Characterisation of Complex Polyethylene Glycol Excipients Using Supercritical Fluid Chromatography-Evaporative Light Scattering Detection-Mass Spectrometry and Comparison with Size Exclusion Chromatography-Triple Detection Array. *J. Chromatogr. A* **2021**, *1638*, 461839. [CrossRef]
9. Cunico, L.P.; Cobo, A.M.; Al-Hamimi, S.; Turner, C. Solubility and Thermal Degradation of Quercetin in CO_2-Expanded Liquids. *Molecules* **2020**, *25*, 5582. [CrossRef]
10. Van Meerten, S.; van Zelst, F.; Tijssen, K.; Kentgens, A. An Optimized NMR Stripline for Sensitive Supercritical Fluid Chromatography-Nuclear Magnetic Resonance of Microliter Sample Volumes. *Anal. Chem.* **2020**, *92*, 13010–13016. [CrossRef]
11. Xhaferaj, M.; Naegele, E.; Parr, M.K. Ion Exchange in Supercritical Fluid Chromatography Tandem Mass Spectrometry (SFC-MS/MS): Application for Polar and Ionic Drugs and Metabolites in Forensic and Anti-Doping Analysis. *J. Chromatogr. A* **2020**, *1614*, 460726. [CrossRef] [PubMed]
12. Papp, D.; Rukkijakan, T.; Lebedeva, D.; Nylander, T.; Sandahl, M.; Samec, J.S.M.; Turner, C. Single-Standard Quantification Strategy for Lignin Dimers by Supercritical Fluid Chromatography with Charged Aerosol Detection. *Anal. Chem.* **2022**, *95*, 1436–1445. [CrossRef]
13. Langley, G.J.; Cancho-Gonzalez, S.; Herniman, J.M. Different Detectors Used with SFC. In *Separation Science and Technology*; Elsevier: Amsterdam, The Netherlands, 2022; Volume 14, pp. 299–324. [CrossRef]
14. Abolhassani, M.; Guais, A.; Chaumet-Riffaud, P.; Sasco, A.J.; Schwartz, L. Carbon Dioxide Inhalation Causes Pulmonary Inflammation. *Am. J. Physiol. -Lung Cell. Mol. Physiol.* **2009**, *296*, L657–L665. [CrossRef]
15. Azuma, K.; Kagi, N.; Yanagi, U.; Osawa, H. Effects of Low-Level Inhalation Exposure to Carbon Dioxide in Indoor Environments: A Short Review on Human Health and Psychomotor Performance. *Environ. Int.* **2018**, *121*, 51–56. [CrossRef]
16. Wilson, A.D. Review of Electronic-Nose Technologies and Algorithms to Detect Hazardous Chemicals in the Environment. *Procedia Technol.* **2012**, *1*, 453–463. [CrossRef]
17. Rambla-Alegre, M.; Tienpont, B.; Mitsui, K.; Masugi, E.; Yoshimura, Y.; Nagata, H.; David, F.; Sandra, P. Coupling Gas Chromatography and Electronic Nose Detection for Detailed Cigarette Smoke Aroma Characterization. *J. Chromatogr. A* **2014**, *1365*, 191–203. [CrossRef]
18. Brenet, S.; John-Herpin, A.; Gallat, F.-X.; Musnier, B.; Buhot, A.; Herrier, C.; Rousselle, T.; Livache, T.; Hou, Y. Highly-Selective Optoelectronic Nose Based on Surface Plasmon Resonance Imaging for Sensing Volatile Organic Compounds. *Anal. Chem.* **2018**, *90*, 9879–9887. [CrossRef] [PubMed]
19. Slimani, S.; Bultel, E.; Cubizolle, T.; Herrier, C.; Rousselle, T.; Livache, T. Opto-Electronic Nose Coupled to a Silicon Micro Pre-Concentrator Device for Selective Sensing of Flavored Waters. *Chemosensors* **2020**, *8*, 60. [CrossRef]

20. Fournel, A.; Mantel, M.; Pinger, M.; Manesse, C.; Dubreuil, R.; Herrier, C.; Rousselle, T.; Livache, T.; Bensafi, M. An Experimental Investigation Comparing a Surface Plasmon Resonance Imaging-Based Artificial Nose with Natural Olfaction. *Sens. Actuators B Chem.* **2020**, *320*, 128342. [CrossRef]

21. Faraco Filho, R.L.; De Castro, J.V.; Barino, F.O.; Campos, D.; Dos Santos, A.B. Enhanced Aroma Prediction in Coffee Fermentation through Optical Fiber Sensor Data Fusion. *Sens. Actuators A Phys.* **2024**, *369*, 115223. [CrossRef]

22. Faraco Filho, R.L.; Oliveira Barino, F.; Calderano, J.; Valle Alvarenga, Í.F.; Campos, D.; Dos Santos, A.B. In-Fiber Mach–Zehnder Interferometer as a Promising Tool for Optical Nose and Odor Prediction during the Fermentation Process. *Opt. Lett.* **2023**, *48*, 3905. [CrossRef] [PubMed]

23. Laplatine, L.; Fournier, M.; Gaignebet, N.; Hou, Y.; Mathey, R.; Herrier, C.; Liu, J.; Descloux, D.; Gautheron, B.; Livache, T. Silicon Photonic Olfactory Sensor Based on an Array of 64 Biofunctionalized Mach-Zehnder Interferometers. *Opt. Express* **2022**, *30*, 33955. [CrossRef]

24. Maho, P.; Herrier, C.; Livache, T.; Comon, P.; Barthelmé, S. Real-Time Gas Recognition and Gas Unmixing in Robot Applications. *Sens. Actuators B Chem.* **2021**, *330*, 129111. [CrossRef]

25. Maho, P.; Herrier, C.; Livache, T.; Rolland, G.; Comon, P.; Barthelmé, S. Reliable Chiral Recognition with an Optoelectronic Nose. *Biosens. Bioelectron.* **2020**, *159*, 112183. [CrossRef]

26. Ashrafi, T.M.S.; Mohanty, G. Surface Plasmon Resonance Sensors: A Critical Review of Recent Advances, Market Analysis, and Future Directions. *Plasmonics* **2025**. [CrossRef]

27. Jia, B.; Chen, J.; Zhou, J.; Zeng, Y.; Ho, H.P.; Shao, Y. Passively and actively enhanced surface plasmon resonance sensing strategies towards single molecular detection. *Nano Res.* **2022**, *15*, 8367–8388. [CrossRef]

28. Cho, S.H.; Choi, S.; Suh, J.M.; Jang, H.W. Advancements in surface plasmon resonance sensors for real-time detection of chemical analytes: Sensing materials and applications. *J. Mater. Chem. C* **2025**, *13*, 6484–6507. [CrossRef]

29. Roy, J.N.; Changder, A.; Mukherjee, K. Design and analysis of ultralow-power all-optical EX-OR and OR logic operations with chiral Mach-Zehnder interferometer. *J. Opt.* **2024**. [CrossRef]

30. Butt, M.A. Surface Plasmon Resonance-Based Biodetection Systems: Principles, Progress and Applications—A Comprehensive Review. *Biosensors* **2025**, *15*, 35. [CrossRef]

31. Stuart, D.D.; Van Zant, W.; Valiulis, S.; Malinick, A.S.; Hanson, V.; Cheng, Q. Trends in Surface Plasmon Resonance Biosensing: Materials, Methods, and Machine Learning. *Anal. Bioanal. Chem.* **2024**, *416*, 5221–5232. [CrossRef]